

EMPIRICAL MODE DECOMPOSITION BASED INTEREST POINT DETECTOR

Jesmin F. Khan, Reza R. Adhami, Sharif M. A. Bhuiyan

Kenneth E. Barner

University of Alabama in Huntsville
Department of ECE
Huntsville, AL 35899, USA

University of Delaware
Department of ECE
Newark, DE 19711, USA

ABSTRACT

A novel method based on Empirical Mode Decomposition (EMD) is introduced in this paper for the detection of affine invariant interest or feature points. The proposed algorithm is a contour based method, where image edges are first detected by utilizing morphological operators followed by an edge thinning process and then the corner or interest points are identified based on the local curvature of the edges. In this work a novel method based on 1-D EMD is formulated to select good discriminative interest points from the edges. The proposed method is compared with four existing approaches that yield good results. The performance is evaluated by employing a criteria known as *repeatability rate*, which evaluates the geometric stability of an interest point detector under different transformations. The results prove the efficacy and superiority of the proposed technique over other schemes in terms of detecting more true corner points.

Index Terms - Empirical mode decomposition, wavelet decomposition, intrinsic mode function, morphological operations.

1. INTRODUCTION

Current interest point detection methods can be categorized into three types: contour based, parametric model based and intensity based methods. Parametric model methods fit a parametric intensity model to the signal [1, 2]. Intensity based methods compute a measure that indicates the presence of an interest point directly from the grey values [3, 4]. Contour based methods first extract contours and then search for maximal curvature or inflexion points along the contour chains, or carry out some polygonal approximation and then search for intersection points [5, 6]. It is reported that the wavelet transform is a robust scheme for feature points detection due to its ability to capture the local deviations at various decomposition levels [7, 8]. Our work is inspired by the fact that there is a correspondence between the wavelet decomposition (WD) and an EMD of a given signal, e.g. WD of a signal gives higher energy where the signal contains information, likewise intrinsic mode function (IMF) of EMD shows higher frequency content at the same locations.

This paper presents a novel affine invariant interest point detector based on 1-D EMD [9]. In addition, a new scheme for edge thinning is proposed. Specifically, edge detection is performed using morphological gradient operator [10], followed by edge thinning based on edge thickness in the horizontal and vertical directions. To detect true corner points from the circular arcs, the 2-D boundaries of an object are represented by the 1-D tangent angles of the boundary point coordinates. Then we use an eigenvector of the covariance matrix for a boundary point over a small region of support (ROS) on a small boundary segment, as a curvature function for feature point detection [11, 8]. Based on the fact that true corners result in stronger

tangent variations, the 1-D EMD is utilized to decompose the 1-D tangent angles and capture the irregular angle variations. Finally, the locations of the true feature points are identified by comparing the local frequency content of the first intrinsic mode function (IMF) of the 1-D decomposed signal with a pre-defined threshold.

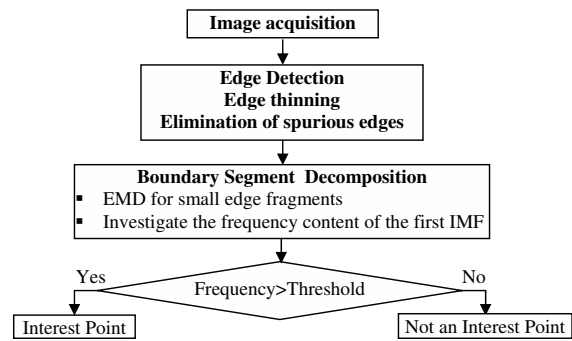


Fig. 1. Block Diagram of the proposed algorithm

In this paper we evaluate the proposed method utilizing the 'repeatability' [12] criteria, which directly measures the quality of the detected feature points for tasks such as image matching, object recognition and 3D reconstruction. Repeatability explicitly compares the geometrical stability of the detected interest points between different images of a given scene taken under varying viewing conditions. The proposed detector is compared to four existing methods which have been shown to yield good results. Utilizing repeatability the proposed method is shown to yield comparable to improved results.

2. PROPOSED ALGORITHM

A block diagram of the proposed algorithm is shown in Fig 1, and the algorithm steps are detailed in the following:

2.1. Morphological Edge Detection

In the followed edge detection scheme, the intensity image I is first blurred (to reduce false edges and over-segmentation) using open-close and close-open filters. The final blurred image, I_b , is the average of the outputs of these two filters. Next, the morphological gradient operator is applied to the blurred image I_b , resulting in an image, $I_{es} = \delta^B(I_b) - \epsilon^B(I_b)$, where δ^B and ϵ^B are the dilation and erosion operators, respectively, utilizing a 3×3 structuring element B . The resulting image I_{es} is then globally thresholded by the level, $\gamma = \sum(I_{es} \cdot c) / \sum c$, where \cdot denotes pixel-wise multiplication and $c = \max(|g_1 * I_{es}|, |g_2 * I_{es}|)$; where, $g_1 = [-101]$;

$g_2 = [-101]^T$, and $**$ denotes 2-D convolution. The binary edge image is given by, $I_e = 1$; if $I_{es} > \gamma$ and $I_e = 0$; if $I_{es} \leq \gamma$. A new edge thinning algorithm is applied to this binary image to obtain fine, narrow and well-defined object boundaries, where the morphological edge map is scanned along the horizontal and vertical directions to reduce the width of the edges to a single pixel by erosion. During horizontal scanning, all the nonzero neighborhood pixels of a nonzero edge pixel in a horizontal window $1 \times w_h$ are set to 0. The resulting image is I_{he} ,

$$\begin{aligned} I_{he}(x_i, y_i) &= I_e(x_i, y_i); \text{ for } I_e(x_i, y_i) \neq 0 \\ I_{he}(x_i, y_j) &= 0; \text{ for } j \in_{j \neq i} \left\{ i - \frac{w_h}{2}, i + \frac{w_h}{2} \right\} \end{aligned} \quad (1)$$

Similar operations in the vertical direction yield

$$\begin{aligned} I_{ve}(x_i, y_i) &= I_e(x_i, y_i); \text{ for } I_e(x_i, y_i) \neq 0 \\ I_{ve}(x_j, y_i) &= 0; \text{ for } j \in_{j \neq i} \left\{ i - \frac{w_v}{2}, i + \frac{w_v}{2} \right\} \end{aligned} \quad (2)$$

The maximum of I_{he} and I_{ve} is set as the thinned binary edge image, $I_{te} = \max(I_{he}, I_{ve})$. The image I_{te} may still contain isolated noisy spurious edges and to remove these, edge segments of length less than N are deleted. Let n sequential points describe an edge segment P in I_{te} such that $P = \{p_i = (x_i, y_i); i = 1, 2, 3 \dots n\}$. Then

$$I_{te}(x_i, y_i) = 0 \text{ for } (x_i, y_i) \in P \text{ and } n \leq N \quad (3)$$

The resulting final binary edge image, I_{fte} , contains 1-pixel width boundaries in the image.

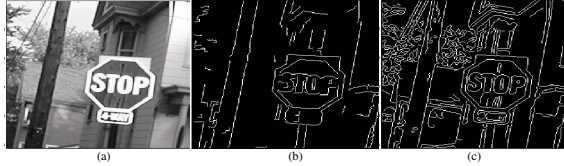


Fig. 2. a) Intensity image, b) Morphological edge image, and c) Canny edge image

The derived edge detection and thinning method is used in lieu of traditional method, such as Canny edge detection [13], because it returns edge segments rather than contiguous edge lines, which is beneficial in feature point detection. As an example, the intensity image, the final morphological edge image and the edge image obtained by Canny's method are shown in Fig 2 (a), (b) and (c), respectively. From this figure it can be seen that the method used in this work yields fewer extraneous boundaries than Canny's method. Furthermore, the proposed method returns all necessary foreground object boundaries.

2.2. Feature Points Extraction

After obtaining the binary edge image, I_{fte} , the feature points along the boundaries of objects must be determined. In this work, the 2-D boundaries of an object are initially transformed to a 1-D $\theta - P$ representation. The procedure of finding the tangent angle of the boundary point is as follows.

2.2.1. 1-D $\theta - p$ Representation of Boundary Segment

From the binary edge image, I_{fte} the x - y coordinates of each point of a boundary segment are first extracted into an array. Let a boundary P of an object be described by n sequential digital points, $P = \{p_i = (x_i, y_i); i = 1, 2, 3 \dots n\}$, where p_{i+1} is adjacent to p_i on P .

Let $N_s(p_i)$ denotes a small boundary segment of P with point p_i is at the center of $N_s(p_i)$ over the ROS between points p_{i-s} and p_{i+s} for some integer s . That is, $N_s(p_i) = \{p_j : j \in \{i - s, i + s\}\}$. Therefore, the covariance matrix $M(p_i)$ for point p_i is estimated by the boundary points coordinates within $N_s(p_i)$ [14]:

$$M(p_i) = \begin{bmatrix} m_{11} & m_{12} \\ m_{21} & m_{22} \end{bmatrix} \quad (4)$$

$$\begin{aligned} m_{11} &= \left[\frac{1}{2s+1} \sum_{j=i-s}^{j=i+s} x_j^2 \right] - \bar{x}_i^2, \quad m_{22} = \left[\frac{1}{2s+1} \sum_{j=i-s}^{j=i+s} y_j^2 \right] - \bar{y}_i^2 \\ m_{12} &= m_{21} = \left[\frac{1}{2s+1} \sum_{j=i-s}^{j=i+s} x_j y_j \right] - \bar{x}_i \bar{y}_i \end{aligned}$$

where \bar{x}_i and \bar{y}_i are the geometrical center of $N_s(p_i)$. The eigenvalues λ_1 and λ_2 of $M(p_i)$ are the solutions of the characteristic equation $DET(M(p_i) - D)$, where D is unit matrix. The tangent angle of point p_i , denoted by $\theta(p_i)$, is simply defined as, $\theta(p_i) = \arctan\left(\frac{\lambda_1 - m_{11}}{m_{12}}\right)$.

2.2.2. Detection Procedure

Consider a n_1 -point digital boundary, $P = \{p_i = (x_i, y_i); i = 1, 2 \dots n_1\}$, traversing points $(x_1, y_1), \dots, (x_{n_1}, y_{n_1})$, and circumventing the boundary in the counterclockwise direction. For each p_i there corresponds a 1-D $\theta - P$ signal, $\theta(p_i)$, 1-D wavelet signal, $Y(p_i)$, and a 1-D first IMF signal of the EMD, $X(p_i)$. As an example we have chosen a binary image of an artificial 'h'-shape object. Fig 3 (a) presents the edge image of that object with one boundary involving $n_1 = 273$ boundary points. The character '+' in Fig 3 (a) denotes the starting boundary point (x_1, y_1) and the arrow indicates the direction of boundary following. The corresponding 1-D $\theta - P$ representation of the object boundary, $\theta(p_i)$ is shown at the top of Fig 3 (b), which is used as an input signal to both the 1-D WD utilizing the 'harr' basis function and the 1-D EMD. The middle plot of Fig 3 (b) shows 1-D wavelet coefficients at the finest (first) detailed decomposition level, $Y(p_i)$. The bottom plot of Fig 3 (b) is the first IMF $X(p_i)$ obtained from $\theta(p_i)$. From Fig 3, it is clearly seen the correspondence between the value of wavelet coefficients and the frequency content of the first IMF. The finest scale wavelet energies are distinctly higher at curvatures than at smooth boundary points. Feature points extracted by the 1-D WD method are shown in Fig 3 (c).

In case of EMD, the first IMF shows distinctly higher frequency content at true feature points than at straight lines. The algorithm for finding true interest points makes four passes through the IMF signal. First, points are selected if they exceed a minimum number of zero crossings around them. Second, if two selected points are adjacent then one is deleted based on the concentration of zero crossings. During third pass, the selected points that are not locally maximum in the original intensity image in its 3×3 neighborhood are deleted. In the final pass, the subset of pixels are kept such that the minimum distance between any pair of points is larger than a given threshold. Let $Z(p_i)$ be the set of zero-crossing points of the IMF around p_i .

$$Z(p_i) = \{p_j : X(p_{j-1})X(p_{j+1}) < 0\} \quad (5)$$

for $j \in \{i - \frac{W_z}{2}, i + \frac{W_z}{2}\}$, where W_z defines window centered at p_i . If for a point the number of zero crossings is greater than a predefined threshold, th_z (in our work the threshold is $1/3$ of the maximum number of zero crossings in the IMF signal), that point is likely a feature point. This is the first selection of the feature points from the object boundary, which forms the set $F_1 \subset P$.

$$\begin{aligned} F_1 &= \{p_i : Z(p_i) > th_z\} \\ F_1 &= \{p_i = (x_i, y_i); i = 1, 2, 3 \dots n_2 : n_2 < n_1\} \end{aligned} \quad (6)$$

where n_1 is the no. of all the boundary points and n_2 is the number of selected points after discarding redundant points. To further discard redundant points from F_1 , we check whether several neighboring points have the same number of zero crossing points over a $W_s=1 \times 11$ size window, and we keep the points among those that has the most concentrated zero crossing points. Hence for each point over the window W_z , we calculate the sum of the distances from all the zero crossing points to the point under consideration, p_i ,

$$S(p_i) = \sum_{j=i-\frac{W_z}{2}}^{j=i+\frac{W_z}{2}} |p_i - p_j|.$$

If $F_2 \subset F_1$ is the set of feature points after discarding redundant points from F_1 , then $\overline{F_2} \cap F_1$ is the set of discarded points.

$$\begin{aligned} \overline{F_2} \cap F_1 &= \{p_j : Z(p_j) = Z(p_i), S(p_j) \neq \min\{S(p_j)\}\} \\ F_2 &= \{p_i = (x_i, y_i); i = 1, 2 \dots n_3 : n_3 < n_2\} \end{aligned} \quad (7)$$

for $j \in \{i - \frac{W_z}{2}, i + \frac{W_z}{2}\}$, where n_3 is the number of selected points after discarding redundant points from F_1 . Finally, from the points in F_2 , we retain those points that are locally maximum in their $W_m=3 \times 3$ neighborhood with the restriction that the distance between any two feature points is larger than a given threshold (this is set to 5 pixels in our experiment). Thus, $F_3 \subset F_2$ is the set of feature points that are locally maximum in the edge image, I_{fte} , and $F_f \subset F_3$ is the final set of feature points after discarding those closely spaced points.

$$\begin{aligned} F_3 &= \{p_i = (x_i, y_i) : I_{fte}(x_i, y_i) = \max I_{fte}(x_j, y_j)\} \\ F_f &= \{p_i = (x_i, y_i); i = 1, 2 \dots n_4 : n_4 < n_3\} \end{aligned} \quad (8)$$

for $j \in \{i - \frac{W_z}{2}, i + \frac{W_z}{2}\}$, where n_4 is the number of selected points after discarding redundant points from F_2 .

$$\begin{aligned} F_f &= \{p_i : |p_i - p_{i-1}| > 5 \text{ pix}, |p_i - p_{i+1}| > 5 \text{ pix}\} \\ F_f &= \{p_i = (x_i, y_i); i = 1, 2, 3 \dots n_5 : n_5 < n_4\} \end{aligned} \quad (9)$$

where n_5 is the number of selected points after discarding redundant points from F_3 . Following the above procedure, the extracted final feature points, F_f for the artificial 'h'-shape object are shown in Fig 3 (d). EMD determined feature points are found at all the curvatures of the object whereas the WD approach misses some curvatures as shown in Figs 3 (c) and (d).

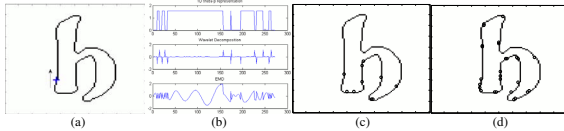


Fig. 3. a) Edge image of letter 'h'; b) The 1-D $\theta - P$ representation (top), haar wavelet decomposition (middle), and the first IMF of EMD (bottom); c) Feature points obtained from wavelet coefficients; and d) Feature points obtained from the frequency content of the first IMF of EMD

For an image with more than one object and objects with complicated shape, we perform EMD on each edge fragment to extract local curvature following the above procedure. Thus we find feature points for each fragment of edge independently and the final feature points are the accumulation of all the points obtained from all the edge boundary segments.

3. EXPERIMENTAL RESULTS

Results of experiments conducted to test the efficacy of the proposed corner detection algorithm are provided in this section. In order to

test the immunity of the proposed algorithm to transformations, the original images are scaled and rotated. Stability to image noise is also tested. Additionally, the repeatability rates of four interest point detectors are compared with the presented method under different image rotation and scale changes. For comparison, we have chosen four detectors that are reported to offer good performance. Among the four chosen detectors, Harris [3] and Tomasi's method [4] are intensity based methods. These are chosen because Harris's method has been reported to be better than any other detector and Tomasi's detector is the best for tracking applications. The other two detectors [7, 8] are chosen because 1) they are contour based methods like the proposed method and 2) they use the WD.



Fig. 4. Feature points detected by a) Harris method, b) Tomasi's method, c) Loupias's technique, d) Yeh's algorithm, and e) Proposed technique; Feature points detected in 40° rotated image by f) Harris method, g) Tomasi's method, h) Loupias's technique, i) Yeh's algorithm, and j) Proposed technique; Feature points detected in 1.5 times scaled image by k) Harris method, l) Tomasi's method, m) Loupias's technique, n) Yeh's algorithm, and o) Proposed technique; Feature points detected in noisy image by p) Harris method, q) Tomasi's method, r) Loupias's technique, s) Yeh's algorithm, and t) Proposed technique

Simulation results of the five methods on real image are presented in Fig 4. For the reference image shown in Fig 2 (a), feature points extracted by Harris's approach, Tomasi's method, Loupias's technique, Yeh's algorithm and the presented method are shown in Fig 4 (a), (b), (c), (d) and (e), respectively. From this figure it can be seen that points selected by the proposed method covers all the curvatures of object boundaries and yields the most true corner points. To evaluate detector rotation invariance, Figs 4 (j) shows the detection results of the proposed method for the rotated version of the reference image, where the rotation angle is 40° . The performance of Harris's, Tomasi's, Loupias's and Yeh's methods are given in Fig 4 (f), (g), (h) and (i), respectively. From the figures, it can be said that Harris's and the proposed method give the best result for this rotation. The performance of Loupias's technique is better than Yeh's algorithm and Tomasi's method is not rotation invariant.

The effect of image scale change on detection result is tested and demonstrated in Figs 4 (k)-(o), where the scale factor is 1.5. Points detected by Harris's, Tomasi's, Loupias's, Yeh's and proposed methods are presented in Fig 4 (k), (l), (m), (n) and (o), respectively. It can be seen from the figures that all the methods are scale invariant. To check the performance with noise, we have added Gaussian noise with a SNR of 25dB. The performance of Harris's, Tomasi's, Loupias's, Yeh's and proposed methods are given in Fig 4 (p), (q),

(r), (s) and (t), respectively. The results show that except Loupias's technique, the other four methods work well in presence of noise.

From the figures it can be concluded that the proposed method can be used as an affine scale and rotation invariant detector. As a qualitative evaluation, the stability and accuracy of the detectors are measured using the repeatability criterion [12]. The repeatability score for a given pair of images is the average number of corresponding points detected in those images under different geometric and photometric transformations. We first compare the detectors for image rotation followed by scale change and additive noise. The repeatability rate as a function of the angle of image rotation (0° and 180°) is displayed in Fig 5 (a). Though the repeatability rate of all the five detectors depend on the rotation angle, from the plots it can be noticed that the proposed method is significantly less dependent on image rotation than the other four methods. Specifically, there is no spike in the repeatability rate plot for the EMD based method, unlike the other methods. This transformation independence is a very important characteristic for any feature point detector.

Fig 5 (b) shows the repeatability rate as a function of scale changes from 1 to 4. The results show that all the detectors are scale sensitive. The Harris and the proposed detectors give the best results, with the repeatability rate a decreasing function of scale change. Tomasi's, Laopious's and Yeh's methods are very sensitive to scale change and the results of these methods are hardly usable. To study repeatability in the presence of image noise, the repeatability rate is displayed as a function of SNR. For performance evaluation with noise, the SNR is varied from 21dB to 35dB and the results are displayed in Fig 5 (c). All the detectors give reasonable results in the additive noise cases, with the exception of the Yeh's method. Notably, the proposed method is the least noise sensitive as it obtains a repeatability rate of nearly 70% for all levels of noise considered.

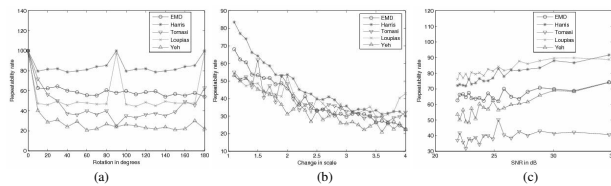


Fig. 5. Plot for the repeatability rate as a function of a) Rotation angle, b) Change in scale, and c) Noise level

After the examination of the overall detection results it can be claimed that the proposed method is better than the other four methods. It's performance is the least dependent on transformations and noise, which is a desirable and attractive characteristic for any feature point detector. As a contour based technique, the presented approach can be expected to perform well for the applications where true corner points are needed to be detected from the object boundaries for further processing.

4. CONCLUSION

In this research, we present a robust, rotation invariant, and scale-invariant corner detection scheme based on the morphological operation, the eigenvectors of covariance matrices and 1-D EMD. We improve the existing morphological edge detection scheme to give thin edges and eliminate spurious edges resulting from the background. The novelty of this work is the utilization of the first IMF of EMD of the 1-D $\theta - P$ signal of the edge to localize true corner points on boundary contours. The interesting attribute of this technique is that it does not detect feature points globally from the whole image

at a time rather it detects feature points locally, based on the neighboring characteristics of a small portion of the edge of an image. That is the reason of the presented method to be more independent of image transformation than the other four methods considered for comparison. Thus, interest points detected by the proposed method are largely independent of the imaging conditions; therefore, points are geometrically stable.

The proposed approach precisely captures the true corner points, has strong robustness of detecting good feature points, and is free from the false alarms on circular arcs for both simple and complicated objects in varying rotation, scale conditions and noise contaminations. Experimental results also suggest that the proposed 1-D EMD based corner detection approach is stable and efficient. The proposed method is a generic concept and can find its application in many matching and recognition problems.

5. REFERENCES

- [1] S. K. Nayar S. Baker and H. Murase, "Parametric feature detection," *Intl. Journal of CV*, vol. 27, no. 1, pp. 27–50, 1998.
- [2] D. Geiger L. Parida and R. Hummel, "Junctions: Detection, classification, and reconstruction," *IEEE Trans. on PAMI*, vol. 20, no. 7, pp. 687–698, 1998.
- [3] C. Harris and M. Stephens, "A combined corner and edge detector," in *Proc. of Alvey Vision Conf.*, 1988, pp. 147–151.
- [4] C. Tomasi and T. Kanade, "Detection and tracking of point features," *Tech. Rep. CMU-CS-91-132, Carnegie Mellon University*, 1991.
- [5] F. Arrebola A. Bandera, C. Urdiales and F. Sandoval, "Corner detection by means of adaptively estimated curvature function," *Electronics Letters*, vol. 36, pp. 124–126, 2000.
- [6] F. Mokhtarian and R. Suomela, "Robust image corner detection through curvature scale space," *IEEE Trans. on PAMI*, vol. 20, no. 12, pp. 1376–1381, 1998.
- [7] S. Bres E. Loupias, N. Sebe and J. M. Jolion, "Wavelet-based salient points for image retrieval," in *Proc. of IEEE Conf. on Image Processing*, 2000.
- [8] C. Yeh, "Wavelet-based corner detection using eigenvectors of covariance matrices," *Pattern Recognition Letters*, vol. 24, pp. 2797–2806, 2003.
- [9] S. R. Long M. C. Wu H. H. Shih Q. Zheng N. Yen C. C. Tung N. E. Huang, Z. Shen and H. H. Liu, "The empirical mode decomposition and the hilbert spectrum for nonlinear and non-stationary time series analysis," in *Proc. of Mathematical, Physical and Engineering Sciences, Royal Society London*, 1998, pp. 903–995.
- [10] K. K. Chin and J. Saniie, "Morphological processing for feature extraction," in *Proceedings of SPIE*, 1993, pp. 288–302.
- [11] H. T. Hou D. M. Tsai and H. J. Su, "Boundary-based corner detection using eigenvalues of covariance matrices," *Pattern Recognition Letters*, vol. 20, pp. 31–40, 1999.
- [12] R. Mohr C. Schmid and C. Bauckhage, "Evaluation of interest point detectors," *Computer Vision, Graphics and Image Processing*, vol. 37, no. 2, pp. 151–172, 2000.
- [13] J. Canny, "A computational approach to edge detection," *IEEE Trans. on PAMI*, vol. 8, no. 6, November 1986.
- [14] R.C. Gonzalez and R.E. Woods, *Digital Image Processing*, Addison Wesley, Massachusetts, 1993.